Journal of Electronic Materials (2024) 53:5159–5168
https://doi.org/10.1007/s11664-024-11185-8

28TH INTERNATIONAL CONFERENCE ON NUCLEAR TRACKS AND RADIATION MEASUREMENTS

ZrO_2 Nanoparticles Synthesized by the Sol–Gel Method: Dependence of Size on pH and Annealing Temperature

Gayatri Shishodia[1] · Shubhra Gupta[2] · Neelam Pahwa[2] · P. K. Shishodia[2]

Received: 17 January 2024 / Accepted: 14 May 2024 / Published online: 7 June 2024

Abstract
Zirconium oxide(ZrO_2) is an important ceramic material characterized by a wide optical bandgap, low optical losses, high dielectric constant, excellent physical and structural properties, high coefficient of thermal expansion and chemical stability. This paper reports the synthesis of ZrO_2 nanoparticles by the sol–gel method using $ZrO(NO_3)_2$ as the zirconium precursor and ammonia solution (25%) as the precipitating agent. The pH value of the sol and the annealing temperature strongly influence the morphology and size of nanoparticles. In the present work, the sol pH was varied from 8 to 11 and the nanoparticles obtained were annealed in the temperature range of 400–700°C. The structural, morphological and optical properties of the nanoparticles were investigated using x-ray diffraction, field-emission scanning electron microscopy, high-resolution transmission electron microscopy, Fourier transform infrared spectroscopy, Raman spectroscopy and photoluminescence measurements. The results demonstrate that the stable t-ZrO_2 phase starts appearing above 400°C, with nanoparticle size varying in the range of 15–22 nm. The optimal size of ZrO_2 nanoparticles (15.65 nm) was obtained at a pH value of 9 and an annealing temperature of 500°C.

Keywords ZrO_2 nanoparticles · $ZrO(NO_3)_2$ · pH · annealing · sol–gel

Introduction

Zirconium oxide (ZrO_2), a transition metal oxide, is widely studied, as it exhibits exceptional physical, chemical, optical, electrical and structural properties.[1–3] ZrO_2, or simply zirconia, is a white crystalline oxide of zirconium that occurs naturally and stabilizes in three crystalline phases: monoclinic, tetragonal and cubic. At room temperature, zirconia has a stable monoclinic (m-ZrO_2)($P2_1/c$) phase.[4] As the temperature increases beyond 1170°C, ZrO_2 transforms into a tetragonal phase (t-ZrO_2)($P4_2/nmc$)[5] and remains stable up to 2370°C. Similarly, its cubic phase (c-ZrO_2)(Fm3 m)[6] is stable at temperatures greater than 2370°C. At room temperature, the optical bandgap varies in the range of 3.25–5.0 eV, and a large number of oxygen vacancies on the ZrO_2 surface result in its *p*-type semiconducting behaviour.[7] In a theoretical study by Goumrhar et al.,[8] it was reported that the nature of the bond between zirconium (Zr) and oxygen (O) is ionic, with electronegative values of 1.33 and 3.44, respectively. The energy bands of ZrO_2 are composed of different proportions of 4d and 2p energy states of Zr and O, respectively. The density of states of ZrO_2 demonstrates that the 2p state of O is dominant below the Fermi level with some combination of 4d Zr energy states, whereas the 4d state of Zr is dominant above the Fermi level with some combination of O 2p energy states.

Wide-bandgap semiconductor materials have garnered considerable research attention for their usefulness in sensing and detection, dielectrics and piezoelectrics for developing advanced technologies.[9–16] The unique band structure and exceptional characteristics of ZrO_2 make it well suited for applications in various domains. The size of energy storage devices such as capacitors was reduced by the fabrication of a metal–insulator–semiconductor (MIS) capacitor structure using Al/ZrO_2/Si for compact electronic applications.[17] ZrO_2 nanoparticles demonstrate excellent efficacy

✉ Shubhra Gupta
shubhragupta09@gmail.com

[1] Department of Physics, Zakir Husain Delhi College, University of Delhi, Delhi 110002, India

[2] Department of Electronics, Zakir Husain Delhi College, University of Delhi, Delhi 110002, India

in the biomedical fields, and can be a game changer the medical and healthcare sectors. The luminescence properties of Tb-ZrO_2 nanoparticles synthesized via a microwave hydrothermal process were evaluated in a murine neuron culture by studying the structural properties of the host lattice. The absorption of additional yttrium atoms into the host ZrO_2 lattice proved to be a viable tool in neuroscience applications.[18] Practical and theoretical studies have also provided new insights into the exploration of ZrO_2 as a catalyst material for degradation of harmful dyes in water bodies to protect aquatic biodiversity. Hydrogen generation by ZrO_2 -loaded ferrites in water-splitting reactions was studied by Bhosale et al.,[19] demonstrating its usefulness in energy production as well. The catalytic activity of ZrO_2 was studied by Raj et al.,[20] who reported that Ag-doped nanoparticles demonstrated better catalytic activity than their undoped counterparts. The wide bandgap of ZrO_2makes it a potential candidate for application in dye-sensitized solar cells (DSSC) as an alternative to conventional materials.[9,21] Co-precipitation,[22] hydrothermal treatment[23] and sol–gel[24] processing are a few of the simplest and lowest-cost methods investigated for the synthesis of ZrO_2 nanoparticles. Among these methods, sol–gel synthesis offers significant advantages, providing excellent chemical homogeneity and higher purity from precursors. By controlling the rate of hydrolysis and condensation reactions, it allows for precise control over morphology and particle size and shape.[25]

The present research work is aimed at exploring the structural, morphological and optical properties of ZrO_2 nanoparticles synthesized via the sol–gel route. Zirconium oxynitrate ($ZrO(NO_3)_2$) and ammonia solution (NH_4OH) were used as the precursor and precipitant, respectively, for the synthesis of ZrO_2 nanoparticles. The effect of pH and annealing temperature on the growth of stabilized ZrO_2 nanoparticles was investigated. The pH-optimized nanoparticles were calcined at different annealing temperatures. X-ray diffraction (XRD), scanning electron microscopy (SEM), high-resolution transmission electron microscopy (HRTEM), Raman spectroscopy, Fourier transform infrared (FTIR) spectroscopy and photoluminescence (PL) were used for characterization of the nanoparticles. The effect of annealing temperature on the crystal phase, particle size, surface morphology, bond structure and defects was also investigated.

Experimental Details

Chemicals and Materials

Reagents used in the experiment including zirconium oxynitrate ($ZrO(NO_3)_2$), ammonia solution(NH_4OH) and acetone were of analytical grade and were utilized without any further purification process. Deionized (DI) water was used as solvent throughout the experiment.

Synthesis

ZrO_2 sols were prepared by dissolving 0.2 M of $ZrO(NO_3)_2$ in DI water on an ultrasonic magnetic stirrer. A clear and transparent solution with no precipitate or turbidity was obtained by continuous stirring for 30 min at room temperature. During stirring, 25% ammonia solution was added drop-wise to adjust the pH value of sol from 8 to 11. The pH-modified sols were continuously stirred for another 30 min. The resulting sols were kept undisturbed for 48 h to facilitate the process of gelation and hydrolysis. A white precipitate settled at the bottom of the flask which was then filtered through Whatman filter paper. During filtering, the precipitate was washed three times in DI water. The washed and filtered powder was then dried completely at 100°C for 120 min. After drying, the crystals were hand-crushed into powder using an agate mortar and pestle. The obtained powder was then annealed at 400°C for 3 h to obtain ZrO_2 nanopowder.

Nanoparticle Characterization

The synthesized nanoparticles were characterized by various characterization techniques including x-ray diffraction (XRD), field-emission scanning electron microscopy (FESEM), energy dispersive x-ray spectrometry (EDS), transmission electron microscopy (TEM), Raman spectroscopy (RS), Fourier transform infrared (FTIR) spectroscopy and photoluminescence (PL). ZrO_2 phases were identified using a Rigaku SmartLab XRD fitted with a copper tube emitting x-rays at $\lambda = 1.5406$ Å with k_α emission lines produced at 40 kV and 30 mA. The samples were scanned in the range of $20° < 2\theta < 80°$ with 0.02° angular steps at 5°/min. Microstructural studies and compositional analysis were performed using a Zeiss Gemini FESEM and EDS. The size and shape of the synthesized nanoparticles were determined using TEM. A Horiba PTI QuantaMaster Series (QM-8540-11-C) setup was used to record the PL emission spectra. A 450 W xenon lamp was used as the excitation source with a 290 nm excitation wavelength. A Thermo Scientific FTIR spectrometer was used to record spectra in the scanning range of 400–4000 cm^{-1} using a KBr pellet. Raman spectra were recorded to determine the vibrational modes of the grown nanopowders in the wavenumber range of 120–1000 cm^{-1}.

Results and Discussion

The crystal structure and phase purity of the synthesized ZrO_2 nanoparticles obtained at different pH and temperature were examined using the x-ray diffraction pattern, as shown in Fig. 1. The solution pH was adjusted from 8 to 11, as precipitation of nanoparticles at lower pH values becomes difficult. The relative intensity and spacing value of the observed peaks were confirmed with JCPDS card no. 80-2155.[26] Diffraction peaks corresponding to (101), (110), (112), (211), (202) and (220) refection planes at $2\theta = 30.18°$, 35.01°, 50.35°, 59.95°, 62.91° and 74.48°, respectively, were indexed to t-ZrO_2 for all the samples prepared at pH values of 8–11. Low-intensity peaks at $2\theta = 28.2°$ and 59.24° correspond to (−111) and (131) diffraction planes, respectively, of the monoclinic phase at pH = 8 and are in good agreement with JCPDS card no. 86-1449.[27,28] The strongest-intensity peak along the preferred orientation at the (101) refection plane confirms the formation of crystalline t-ZrO_2.

The crystallite size (D) was calculated using the Debye–Scherrer formula[29]

$$D = \frac{0.94\lambda}{\beta \cos(\theta)}$$

where λ is the Cukα wavelength (1.5406 Å), β is the full width at half maximum (FWHM) and Θ is the half angle corresponding to the strongest-intensity peak. The crystallite size as a function of pH value is plotted in Fig. 1b. It was observed that as pH increases from 8 to 9, the crystallite size decreases by ~27% from 21.56 nm to 15.65 nm. At pH = 10, no significant change in size is observed. At pH = 11, the crystallite size decreases slightly to 14.03 nm. Similar

Table I Crystallite size, microstrain and lattice parameters obtained at different pH values from XRD plots

pH	Crystallite size (nm)	Micro-strain ($\times 10^{-3}$)	Lattice parameters (Å)		
			a	b	c
8	21.565843	2.85	0.457498	0.480752	0.480752
9	15.657236	0.0989	0.459048	0.483456	0.483456
10	15.940893	1.29	0.459587	0.484072	0.484072
11	14.301347	2.06	0.459545	0.484013	0.484013

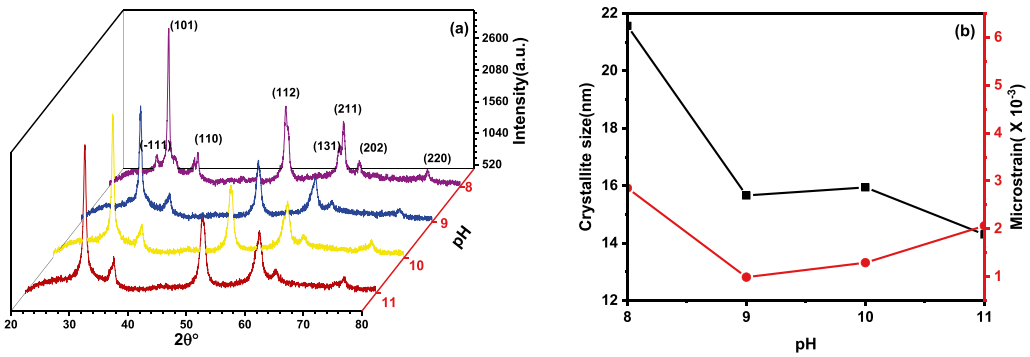

Fig. 1 (a) XRD pattern and (b) variation in crystallite size and microstrain with pH values at 500°C.

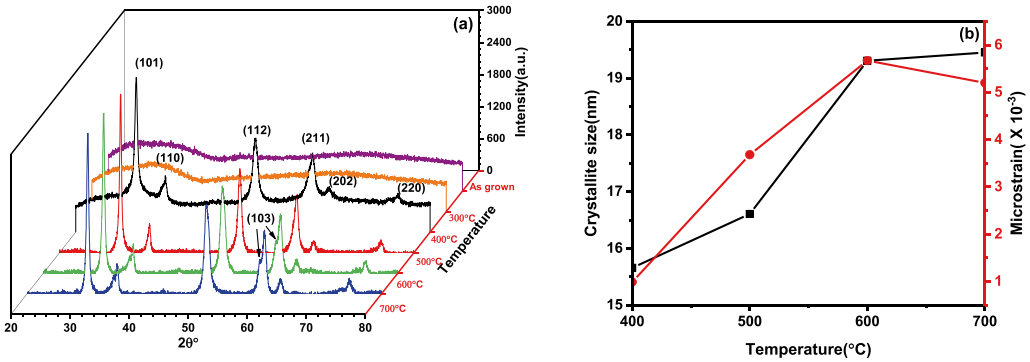

Fig. 2 (a) XRD pattern and (b) variation in crystallite size and microstrain with temperature for a pH value of 9.

observations were reported by Haibo et al.[30] Since highly basic sol does not show much improvement in particle size, nanoparticles grown at pH = 9 can be considered for temperature analysis. The microstrain arising from peak broadening was calculated using Williamson–Hall (WH) plots for all the samples, as shown in Fig. 1b. Positive and negative strain values indicate tensile and compressive strain, respectively. Table I summarizes the calculated results. Lattice parameters were calculated using Eq. 1 as follows.

$$\frac{1}{d_{hkl}} = \frac{h^2}{a^2} + \frac{k^2}{b^2} + \frac{l^2}{c^2} \tag{1}$$

Lowest strain was found at pH = 9. This can be attributed to the fact that the average crystallite size is strongly dependent on the rate of hydrolysis in the sol–gel process. The route to ZrO_2 nanoparticle synthesis is presented in the following equations.[31]

Table II Crystallite size, microstrain and lattice parameters obtained at different annealing temperatures

Temperature (°C)	Crystallite size (nm)	Microstrain ($\times 10^{-3}$)	Lattice parameters (Å)		
			a	*b*	*c*
400	15.657236	0.0989	0.459048	0.483456	0.483456
500	16.605392	3.68	0.459881	0.484496	0.484496
600	19.305824	5.67	0.459348	0.483873	0.483873
700	19.451929	5.2	0.459794	0.484414	0.484414

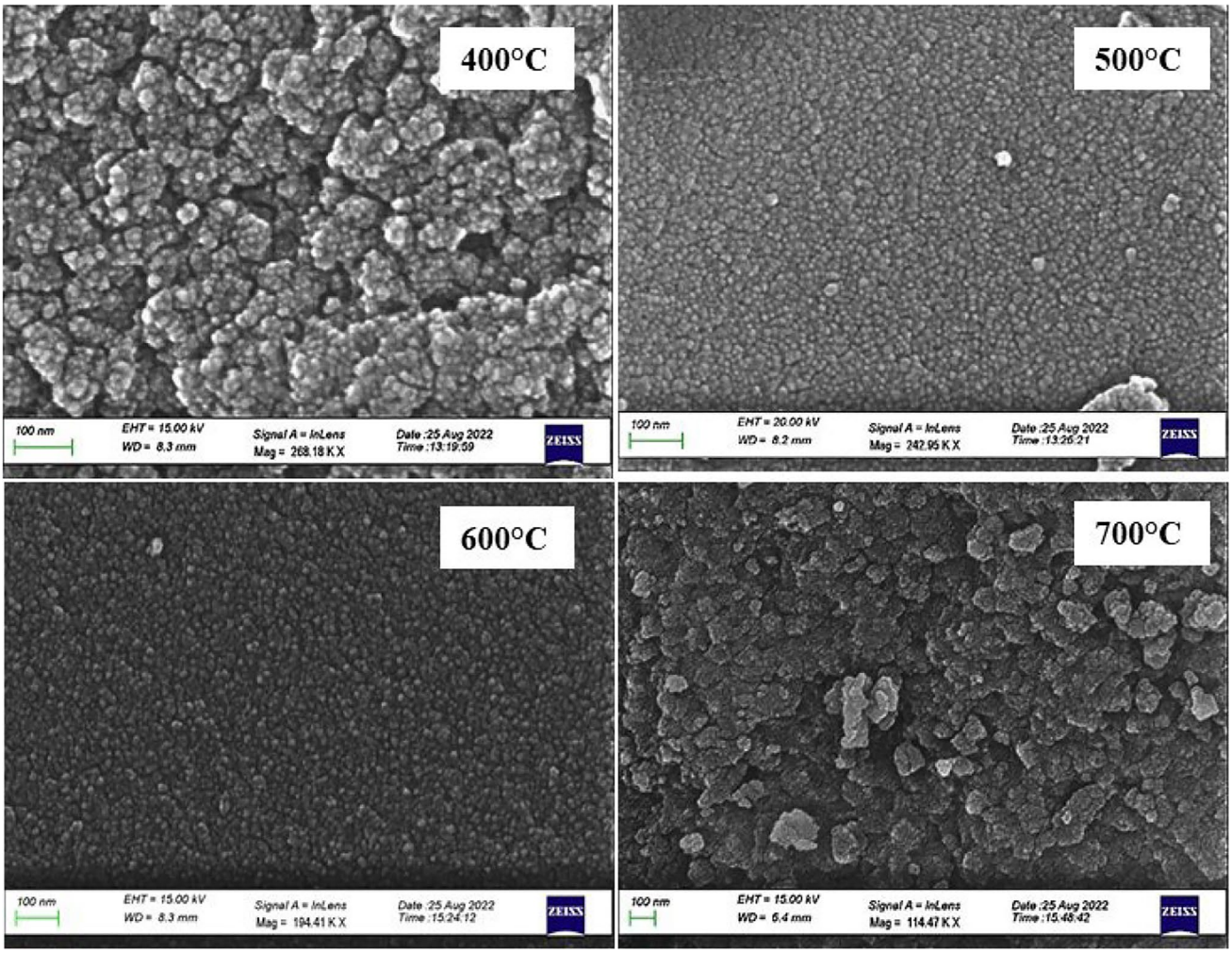

Fig. 3 FESEM images of ZrO_2 nanoparticles annealed at different temperatures.

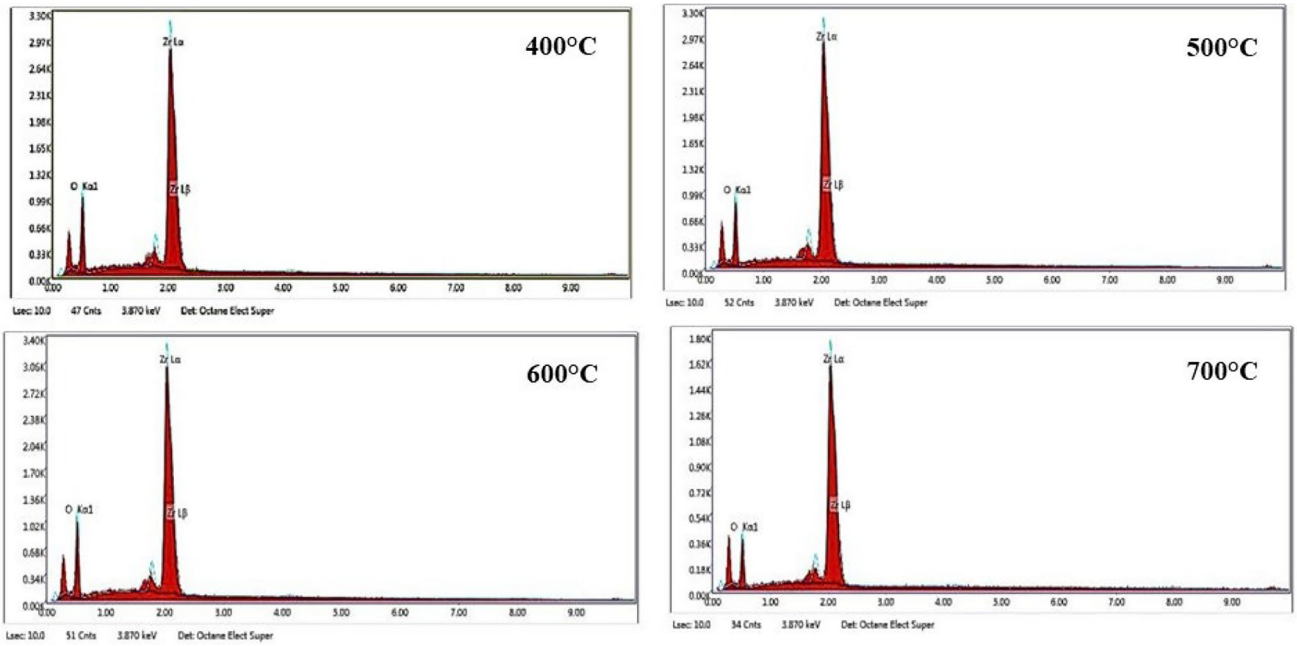

Fig. 4 EDS spectra for ZrO_2 nanoparticles annealed at different temperatures.

Table III Atomic percent of respective elements for the ZrO_2 nanoparticles annealed at different temperatures

Annealing temperature (°C)	Element	Atomic %
400	Zr	27.64
	O	72.36
500	Zr	29.45
	O	70.55
600	Zr	27.64
	O	72.36
700	Zr	34.40
	O	65.60

$$ZrO(NO_3)_2 \rightarrow ZrO^{2+} + 2NO_3^- \quad (2)$$

$$ZrO^{2+} + H_2O \rightarrow Zr(OH)_2^{2+} \quad (3)$$

$$Zr(OH)_2^{2+} + OH^- \rightarrow Zr(OH)^{3+} \quad (4)$$

$$Zr(OH)_3^+ \rightarrow ZrO_2 + H_3O^+ \quad (5)$$

The effect of annealing temperature on ZrO_2 nanoparticles was also investigated, as shown in Fig. 2. Based on the results obtained at different pH values, nanoparticles were synthesized at pH 9 and annealed at temperatures in the range of 300–700°C for 3 h. Phases corresponding to t-ZrO_2 began to appear at 400°C, and the diffraction peaks intensified as the temperature gradually increased. At higher temperatures, a peak indexed at the (103) diffraction plane also appeared.[32] As expected, the Scherrer equation shows the increase in nanoparticle size from 15.65 nm to 19.45 nm (Fig. 2a) with annealing temperature. The variation in microstrain with temperature as computed by WH plots is shown in Fig. 2b. At 700°C, the strain transitioned from tensile to comprehensive, which can be attributed to lattice distortion due to the increase in particle size with temperature.[33]

It can be observed from Table II that the optimized t-ZrO_2 nanoparticles obtained under the present experimental conditions are comparable in size (15.65 nm) to those reported using the hydrothermal process.[34,35] Lattice parameters were found to be consistent with the reported results.[36]

The influence of annealing temperature on the morphology and elemental composition of the synthesized nanoparticles was determined using FESEM and EDS. Figure 3 shows the micrographs for the samples annealed at different temperatures. Spherical morphology can be seen at all temperatures.[37] The average diameter of the nanoparticles varies from 15 nm to 22 nm, which is consistent with XRD calculations. Homogeneous distribution of nanoparticles was observed at 500°C. On further increasing the temperature to 700°C, nanoparticles start to agglomerate, which suggests that the temperature has a significant effect on particle morphology and size distribution.[32]

Energy-dispersive x-ray spectroscopy is a well-known technique used to determine the elemental composition of

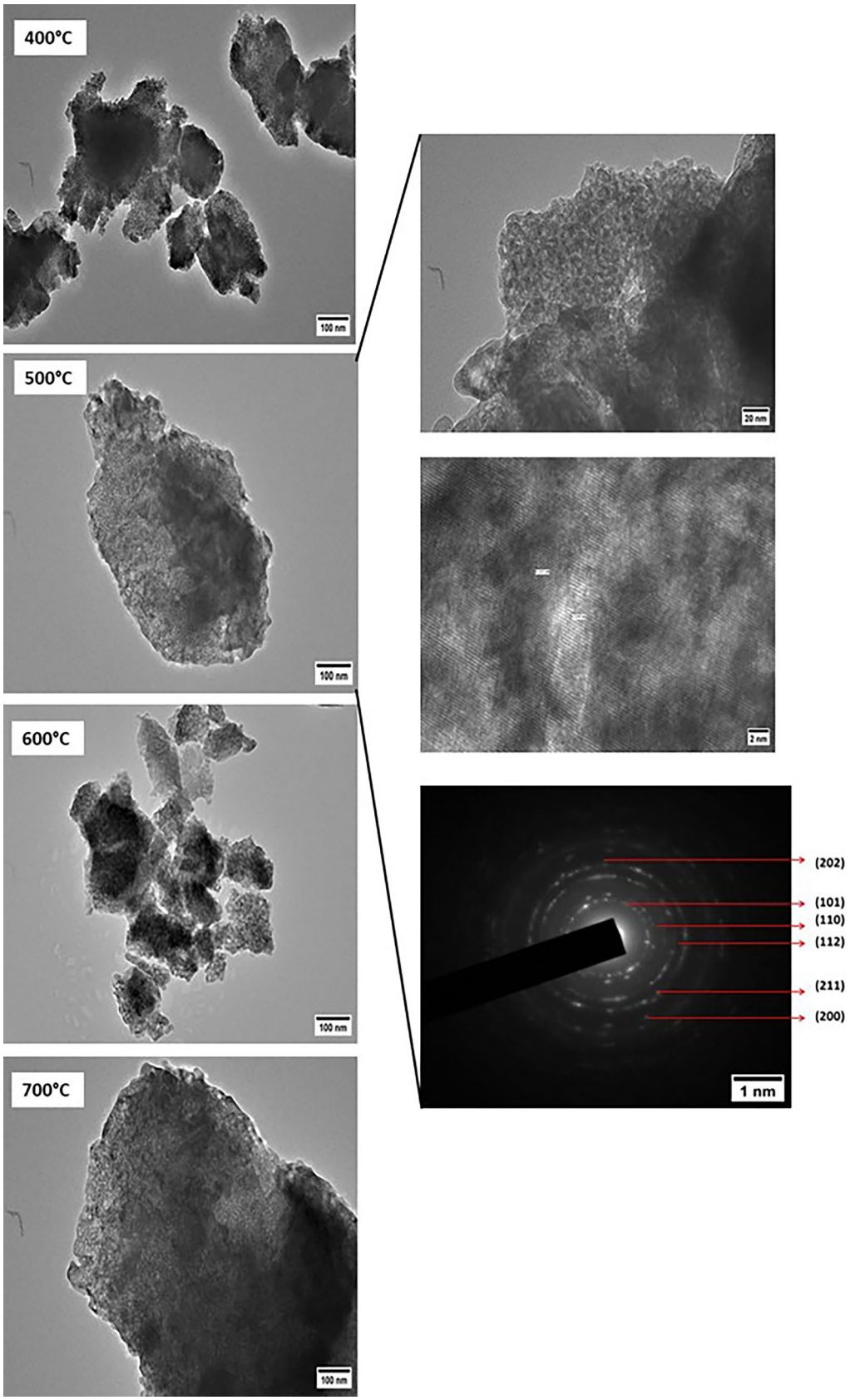

Fig. 5 TEM images of ZrO_2 nanoparticles at different annealing temperatures.

nanoparticles. The EDS spectra for ZrO_2 nanoparticles as depicted in Fig. 4 confirm the presence of Zr and O at all temperatures, with no additional impurities. An appropriate stoichiometric ratio at 500°C indicates that a temperature of 500°C is essential for the growth of ZrO_2 nanoparticles. Table III summarizes the atomic percent of respective elements for the samples annealed at different temperatures for a pH value of 9.

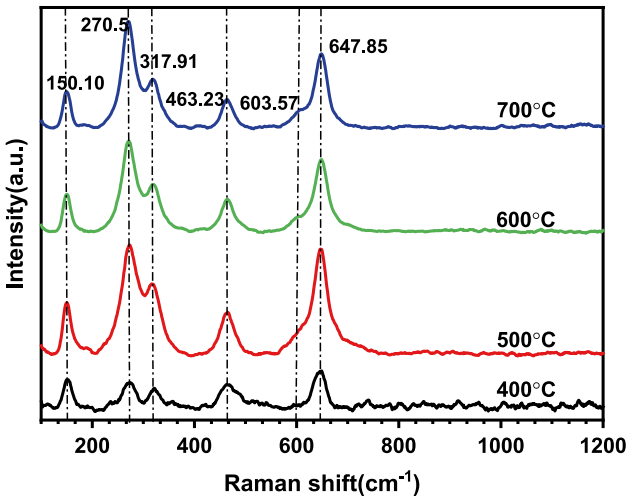

Fig. 6 Raman spectra of ZrO_2 nanoparticles annealed at different temperatures.

Figure 5 shows the TEM micrographs of samples with different annealing temperatures in the range of 400–700°C. Agglomerates of spherically shaped particles are observed. The atomic structure was examined using selected area electron diffraction (SAED) patterns of ZrO_2 nanopowder as shown for samples annealed at 500°C. The acquired images depict a highly crystalline nature of the synthesized particles, and the TEM results appear to be consistent with the XRD results.

Raman spectroscopy is a characterization technique used to examine the vibrational transitions, composition, phase purity and presence of defects in a material. The results of Raman-active vibrational modes for ZrO_2 nanoparticles annealed at different temperatures in the spectral range of 120–1200 cm^{-1} are shown in Fig. 6. The intensity of Raman peaks is greatest for the samples annealed at 500°C. Lopez et al.[38] summarized the Raman-active optical modes for ZrO_2 nanopowder in their study. For the tetragonal phase, ZrO_2 exhibits six active optical modes, $A_{1g}+2B_{1g}+3E_g$, belonging to D_{4h}. For annealed nanoparticles, six Raman-active bands around 150 cm^{-1}, 270 cm^{-1}, 317 cm^{-1}, 463 cm^{-1}, 603 cm^{-1} and 647 cm^{-1} are observed, which is consistent with the literature.[38] Characteristic peaks of A_{1g} at 603 cm^{-1} and E_g at 640 cm^{-1} are ascribed to symmetric and asymmetric stretching of Zr–O–Zr vibrational modes, respectively. Partial symmetric coupling of the A_1 mode results in a peak at 317 cm^{-1}. Similarly, the appearance of

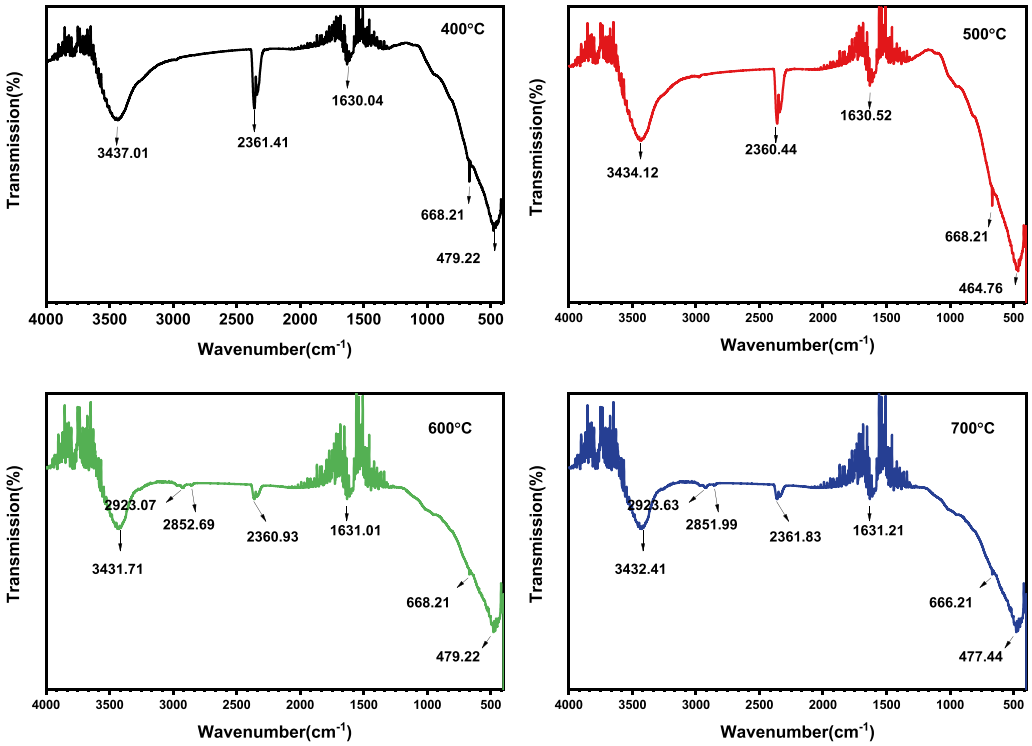

Fig. 7 FTIR spectra of ZrO_2 nanoparticles annealed at different temperatures.

a peak at 463 cm^{-1} is a result of partial symmetric coupling of B_1 and B_2 modes. The peaks identified at 150 (B_{1g}) and 270 (E_g) are due to zirconium ionic vibrations. The peaks recorded at all the annealed temperatures confirm the formation of tetragonal zirconia and are in agreement with the results of FTIR discussed below.

FTIR aids in the analysis of material composition and functional groups present in the structure of the synthesized nanoparticles. Figure 7 displays the FTIR spectra of the annealed nanoparticles in the spectral region 400–4000 cm^{-1}. The region below 1500 cm^{-1} is unique to the material, and the region above provides information on the functional groups present.[37] The characteristic stretching of Zr–O bands around 479 cm^{-1} confirms the formation of t-ZrO_2 at all temperatures. Vibrational stretching around 621 cm^{-1} is due to asymmetrical arrangement of Zr–O–Zr linkages.[39] The adsorption bands at 1630 cm^{-1} and 2361 cm^{-1} indicate the stretching mode of the O–H functional group.[40] Also, the wide adsorption band around 2800–400 cm^{-1} corresponds to the O–H stretching vibrations of the absorbed hydroxyl, indicating that the solvent used to prepare the nanoparticles is ultrapure.[7,40–42] The presence of characteristic peaks indicates the synthesis of ZrO_2 nanoparticles at all the annealing temperatures.

Figure 8 reveals the PL spectra of annealed ZrO_2 nanoparticles recorded using a 290 nm excitation wavelength. The maximum intensity peak for ZrO_2 nanopowder annealed at 400°C is centred at 401 nm (3.09 eV), which corresponds to violet emission, i.e. at the interface of the UV and visible regions. This can be attributed to a near-band-edge emission transition and high crystal quality of the grown nanoparticles. An additional emission peak centred at 429 nm (2.89 eV) is observed at 500°C. The photoluminescence characteristics of ZrO_2 nanoparticles can be examined by observing emission intensities resulting from recombination of photoinduced holes and electrons that are captured by defects. The large surface area of ZrO_2 nanoparticles results in oxygen and zirconium vacancies/interstitial defect centres or point defects.[43] Electrons excited by absorption of high-energy photons are captured by these oxygen vacancies, resulting in the creation of defects in the lattice. After a relaxation process, the electrons undergo a radiative transition that results in various emission wavelengths and intensities.[44] The broad emission band at 600°C is due to the increase in defects as the depletion of grains is more pronounced at higher annealing temperatures. However, on further increasing the temperature to 700°C, a blue shift in the emission band is observed.

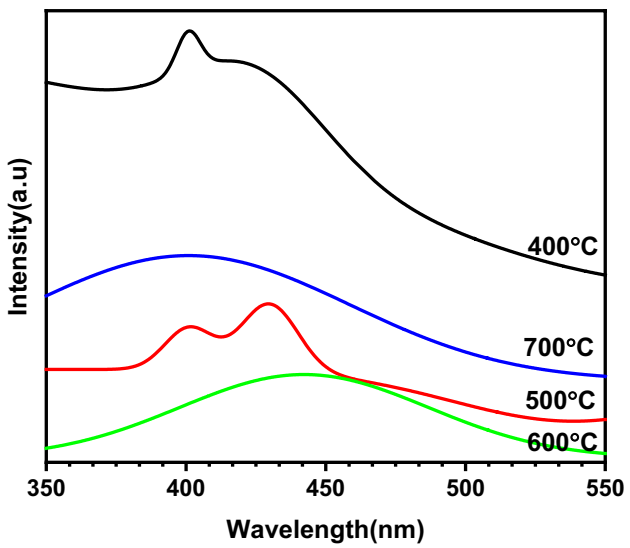

Fig. 8 PL spectra of ZrO_2 nanoparticles annealed at different temperatures.

Conclusion

ZrO_2 nanoparticles were successfully synthesized using the simple and low-cost sol–gel technique. The sol pH was varied from 8 to 11 followed by annealing of the obtained nanoparticles in the temperature range of 400–700°C. These nanoparticles were then investigated for their structural, morphological and optical properties at different annealing temperatures. XRD peaks demonstrated the formation of pure crystalline t-ZrO_2 above 400°C that remained stable at room temperature. The optimal size of 15.65 nm was obtained by using $Zr(NO_3)_2$ as the precursor solution at a pH value of 9 and an annealing temperature of 500°C. FESEM images showed that the particles started to agglomerate as the annealing temperature was increased to 700°C. The SAED pattern obtained at pH 9 and temperature of 500°C confirmed the crystalline nature of the ZrO_2 nanoparticles. No strong influence of annealing temperature was found on vibrational modes, as determined from FTIR and Raman spectra. The presence of oxygen vacancies and lattice distortion above 500°C was confirmed by photoluminescence spectra. These results demonstrate that ZrO_2 nanoparticles obtained by the sol–gel technique can be used for solar cell applications.

Acknowledgments The authors wish to thank the University Science Instrumentation Centre, University of Delhi, Delhi, and Advanced Instrumentation Research Facility at Jawaharlal Nehru University, New Delhi, for providing characterization facilities.

Funding The authors did not receive support from any organization for the submitted work.

Data Availability The authors confirm that the data supporting the findings of this study are available within the article.

Conflict of interest The authors declare no competing interests.

References

1. L. Chouhan and S.K. Srivastava, A comprehensive review on recent advancements in D0 ferromagnetic oxide materials. *Mater. Sci. Semicond. Process.* 147, 106768 (2022).
2. R.O. Ijeh, C.O. Ugwuoke, E.B. Ugwu, S.O. Aisida, and F.I. Ezema, Structural, optical and magnetic properties of Cu-doped ZrO_2 films synthesized by electrodeposition method. *Ceram. Int.* 48, 4686 (2022).
3. Y.L. Yang, X.L. Fan, C. Liu, and R.X. Ran, First principles study of structural and electronic properties of cubic phase of ZrO_2 and HfO_2. *Phys. B Condens. Matter.* 434, 7 (2014).
4. J.D. McCullough and K.N. Trueblood, The crystal structure of baddeleyite (Monoclinic ZrO_2). *Acta Crystallogr.* 12, 507 (1959).
5. G. Teufer, The crystal structure of tetragonal ZrO_2. *Acta Crystallogr.* 15, 1187 (1962).
6. D.K. Smith and C.F. Cline, Verification of existence of cubic zirconia at high temperature. *J. Am. Ceram. Soc.* 45, 249 (1962).
7. W. Ahmed and J. Iqbal, Effect of Ni doping on structural, optical and magnetic characteristics of ZrO_2 nanoparticles with efficient visible light driven photocatalytic activity. *Ceram. Int.* 47, 24895 (2021).
8. F. Goumrhar, L. Bahmad, O. Mounkachi, and A. Benyoussef, Ferromagnetism in Mn and Fe doped ZrO_2 by Ab-initio calculations. *Comput. Condens. Matter.* 19, e00361 (2019).
9. X. Yang, L. Zhao, K. Lv, B. Dong, and S. Wang, Enhanced efficiency for dye-sensitized solar cells with ZrO_2 as a barrier layer on TiO_2 nanofibers. *Appl. Surf. Sci.* 469, 821 (2019).
10. T. Guo, H. Wu, X. Su, Q. Guo, and C. Liu, Surface functionalization toward top-gated monolayer MoS_2 field-effect transistors with ZrO_2/Al_2O_3 as composite dielectrics. *J. Alloys Compd.* 871, 159116 (2021).
11. R. Vaßen, D.E. Mack, M. Tandler, Y.J. Sohn, D. Sebold, and O. Guillon, Unique performance of thermal barrier coatings made of yttria-stabilized zirconia at extreme temperatures (>1500°C). *J. Am. Ceram. Soc.* 104, 463 (2021).
12. N. Shimosako and H. Sakama, Basic photocatalytic activity of ZrO_2 thin films fabricated by a sol–gel method under UV-C irradiation. *Thin Solid Films* 732, 138786 (2021).
13. S.Y. Sokovnin, N. Pizurova, V.G. Ilves, P. Roupcová, M.G. Zuev, M.A. Uimin, M.V. Ulitko, and O.A. Svetlova, Properties of ZrO_2 and Ag–ZrO_2 nanopowders prepared by pulsed electron beam evaporation. *Ceram. Int.* 48, 17703 (2022).
14. M. Huang, T. Liu, F. Sun, and C. Wu, Pt–Co nanoparticles anchored by ZrO_2 for highly efficient and durable oxygen reduction reaction in H_2-air fuel cells. *Int. J. Hydrogen Energy* 47, 22993 (2022).
15. G. Feng, Y. Che, S. Wang, S. Wang, J. Hu, J. Xiao, C. Song, and L. Jiang, Sensitivity enhancement of In_2O_3/ZrO_2 composite based acetone gas sensor: a promising collaborative approach of ZrO_2 as the heterojunction and dopant for in-situ grown octahedron-like particles. *Sens. Actuators B Chem.* 367, 132087 (2022).
16. J.Y. Seo, D. Oh, D.J. Kim, K.M. Kim, and J.S. Kwon, Enhanced mechanical properties of ZrO_2-Al_2O_3 dental ceramic composites by altering Al_2O_3 form. *Dent. Mater.* 36, e117 (2020).
17. M.L. Matias, E. Carlos, R. Branquinho, H.D. Valle, J. Marcelina, M. Morais, A. Pimentel, J. Rodrigues, T. Monteiro, E. Fortunato, R. Martins, and D. Nuens, A comparison between solution-based synthesis methods of ZrO_2 nanomaterials for energy storage applications. *Energies* 15, 6452 (2022).
18. A. Słońska, J. Kaszewski, E. Wolska-Kornio, B. Witkowski, E. Wachnicki, V. Mijowska, Z. Karakitsou, M. Godlewski, M. Gajewski, and M.M. Godlewski, Luminescent properties of ZrO_2: Tb nanoparticles for applications in neuroscience. *Opt. Mater. (Amst)* 59, 96 (2016).
19. R.R. Bhosale, R.V. Shende, and J.A. Puszynski, Sol–gel derived $NiFe_2O_4$ modified with ZrO_2 for hydrogen generation from solar thermochemical water-splitting reaction. *Mater. Res. Soc. Symp. Proc.* 1387, 34 (2011).
20. S. Raj, M. Hattori, and M. Ozawa, Ag-doped ZrO_2 nanoparticles prepared by hydrothermal method for efficient diesel soot oxidation. *Mater. Lett.* 234, 205 (2019).
21. M. Abrari, M. Ahmadi, H.M. Chenari, and M. Ghanaatshoar, Investigating the effect of ZrO_2 nanofibers in ZnO-based photoanodes to increase dye-sensitized solar cells (DSSC) efficiency: inspecting the porosity and charge transfer properties in ZnO/ZrO_2 nanocomposite photoanode. *Opt. Mater. (Amst)* 147, 114690 (2024).
22. H. Wang, H. Huang, J. Liang, and J. Liu, Preparation of ZrO_2/Gd_2O_3 composite ceramic materials by coprecipitation method. *Ceram. Int.* 40, 3995 (2014).
23. S. Sagadevan, J. Podder, and I. Das, Hydrothermal synthesis of zirconium oxide nanoparticles and its characterization. *J. Mater. Sci. Mater. Electron.* 27, 5622 (2016).
24. H. Qin, W. Guo, J. Liu, and H. Xiao, Size-controlled synthesis of spherical ZrO_2 nanoparticles by reverse micelles-mediated sol–gel process. *J. Eur. Ceram. Soc.* 39, 3821 (2019).
25. C. Jeffrey Brinker, George W. Scherer, sol-gel science: the physics and chemistry of sol–gel processing - Google Books, https://books.google.co.in/books?hl=en&lr=&id=CND1BAAAQBAJ&oi=fnd&pg=PP1&ots=afyJI5_jjA&sig=tNA3Rda1-fY508PR7Vc_O_9rCRw&redir_esc=y#v=onepage&q&f=false
26. W. Ahmed and J. Iqbal, Mn doped ZrO_2 nanoparticles: an optically tuned photocatalyst with superior structural magnetic and dielectric characteristics. *J. Phys. Chem. Solids* 160, 110285 (2022).
27. O. Mangla and S. Roy, Monoclinic zirconium oxide nanostructures having tunable band gap synthesized under extremely non-equilibrium plasma conditions in proceedings of IOCN (2018), p 10
28. Z. Zhao and Y. Wang, The synthesis and afterglow luminescence properties of a novel red afterglow phosphor: ZrO_2:Sm^{3+}, Sn^{4+}. *J. Lumin.* 132, 2842 (2012).
29. A. West, *Solid state chemistry and its applications*, 2 Student Edition, (Hoboken: Wiley, 2014), p.584.
30. H. Ouyang, C. Li, K. Li, H. Li, and Y. Zhang, Effect of PH on crystallization of nanocrystalline zirconia in a microwave-hydrothermal process. *J. Wuhan Univ. Technol-Mat. Sci. Edit.* 31, 68 (2016).
31. L. Gal-Or, I. Silberman, and R. Chaim, Electrolytic ZrO_2 coatings: I electrochemical aspects. *J. Electrochem. Soc.* 138, 1939 (1991).
32. W. Huang, H. Qiu, Y. Zhang, L. Nan, L. Gao, J. Chen, M. Omran, and G. Chen, Preparation of nano zirconia by binary doping: effect of controlled sintering on structure and phase transformation. *Ceram. Int.* 48, 25374 (2022).
33. G. Xu, Y.W. Zhang, B. Han, M.J. Li, C. Li, and C.H. Yan, Unusual calcination temperature dependent tetragonal-monoclinic transitions in rare earth-doped zirconia nanocrystals. *Phys. Chem. Chem. Phys.* 5, 4008 (2003).
34. Y. Zhao, L. Xu, M. Guo, Z. Li, T. Wang, Z. Xu, J. Ye, and S. Wei, Effect of triethanolamine on the crystallization behavior and kinetics of nano T-ZrO_2 synthesized by microwave-assisted hydrothermal method. *Ceram. Int.* 47, 26197 (2021).
35. M. Guo, G. Wang, Y. Zhao, H. Li, K. Tang, Y. Zhao, and K. Burgess, Preparation of nano-ZrO_2 powder via a microwave-assisted hydrothermal method. *Ceram. Int.* 47, 12425 (2021).
36. Q. Cheng, W. Yang, Q. Chen, J. Zhu, D. Li, L. Fu, and L. Zhou, Fe-doped zirconia nanoparticles with highly negative conduction

band potential for enhancing visible light photocatalytic performance. *Appl. Surf. Sci.* 530, 147291 (2020).
37. L.S.R. Yadav, T. Ramakrishnappa, J.R. Pereira, R. Venkatesh, and G. Nagaraju, Electrical property of zirconium oxide nanoparticle synthesized by hydrothermal method. *Mater. Today Proc.* 49, 686 (2022).
38. E. Fernandez Lopez, V. Sanchez Escribano, M. Panizza, M.M. Carnasciali, and G. Busca, Vibrational and electronic spectroscopic properties of zirconia powders. *J. Mater. Chem.* 11, 1891 (2001).
39 S.W. Lee and R.A. Condrate, The infrared and raman spectra of ZrOa-SiO_2 glasses prepared by a sol–gel process. *J. Mater. Sci.* 23, 2951 (1988).
40. L. Song, J. Li, H. Zhou, Y. Lin, H. Ding, Y. Huang, P. Zhang, X. Lai, G. Liu, and Y. Fan, Zirconia nano-powders with controllable polymorphs synthesized by a wet chemical method and their phosphate adsorption characteristics & mechanism. *Ceram. Int.* 48, 6591 (2022).
41. A. Aytimur, I. Uslu, S. Koçyiğit, and F. Özcan, Magnesia stabilized zirconia doped with boron Ceria and Gadolinia. *Ceram. Int.* 38, 3851 (2012).
42. N.Y. Mostafa, Z.I. Zaki, Q. Mohsen, S.H. Alotaibi, A.A. El-moemen, and M.A. Amin, Carboxylate-assisted synthesis of highly-defected monoclinic zirconia nanoparticles. *J. Mol. Struct.* 1214, 128232 (2020).
43. L. Kumari, W.Z. Li, J.M. Xu, R.M. Leblanc, D.Z. Wang, Y. Li, H. Guo, and J. Zhang, Controlled hydrothermal synthesis of zirconium oxide nanostructures and their optical properties. *Cryst. Growth Des.* 9, 3874 (2009).
44. I.J. Berlin, V.S. Anitha, P.V. Thomas, and K. Joy, Influence of oxygen atmosphere on the photoluminescence properties of sol–gel derived ZrO_2 thin films. *Solgel. Sci. Technol.* 64, 289 (2012).